Springer

Acta Mechanica Sinica

CrossMark click for updates

• RESEARCH PAPER •

Acta Mech. Sin., Vol. 41, 524208 (2025)
https://doi.org/10.1007/s10409-024-24208-x

Optimal design and dynamic performance analysis of HMDV suspension based on bridge network

Xiaofeng Yang[1,2,3], Yan Yan[1], Yujie Shen[1*], Xiaofu Liu[4], and Zhipeng Wang[5,6]

[1] *School of Automotive and Traffic Engineering, Jiangsu University, Zhenjiang 212013, China;*
[2] *State Key Laboratory of Advanced Design and Manufacturing Technology for Vehicle, Changsha 410012, China;*
[3] *Jiangsu Province and Education Ministry Co-sponsored Synergistic Innovation Center of Modern Agricultural Equipment, Zhenjiang 212013, China;*
[4] *College of Engineering, China Agricultural University, Beijing 100083, China;*
[5] *State Key Laboratory of Intelligent Agricultural Power Equipment, Luoyang 471039, China;*
[6] *Luoyang Tractor Research Institute Co. Ltd., Luoyang 471039, China*

Received July 13, 2024; accepted October 23, 2024; published online January 10, 2025

In order to solve the vertical vibration negative effect problem caused by the increase of the unsprung mass in the hub motor driven vehicle (HMDV), a novel mechatronic suspension using the bridge electrical network is proposed. Firstly, the bridge electrical networks composed of two capacitors, two inductors, and one resistor are summarized and their impedance functions are analyzed forward through the structural method. Then a quarter HMDV model is constructed, and the optimal element parameters in the electrical networks are selected through the Pattern Search algorithm. The influence of element parameters perturbation of the optimal structure on the output response of HMDV suspension is further analyzed. Results show that the proposed bridge electrical network can be realized as a biquartic impedance. It can be equivalent to a mechanical impedance of the suspension through a linear motor. Compared with the conventional suspension, the root-mean-square values of the dynamic tire load and the suspension working space are reduced by 10.76% and 18.10%, respectively. The vibration at low and high frequencies of the unsprung mass is suppressed, effectively improving the grounding and handling stability of the vehicle.

Bridge network, Biquartic impedance, HMDV, Negative effects of vertical vibration

Citation: X. Yang, Y. Yan, Y. Shen, X. Liu, and Z. Wang, Optimal design and dynamic performance analysis of HMDV suspension based on bridge network, Acta Mech. Sin. 41, 524208 (2025), https://doi.org/10.1007/s10409-024-24208-x

1. Introduction

Electric vehicles play a vital role in sustainable mobility. It is estimated that by 2030, battery-electric vehicles will become the mainstream of passenger vehicle transport [1]. The hub-driven technology offers several significant benefits to overcome the challenges in transportation electrification. As an ideal configuration for future electric vehicles, the hub motor driven vehicle (HMDV) has the advantages of high transmission efficiency and flexible operation. The motor is arranged directly in the wheel hub, and the output torque of the motor can be distributed independently so that the handling stability of the vehicle can be improved. Through the independent and accurate control of the motor, the control of the vehicle's driving dynamics becomes faster and easier [2]. Despite the many advantages of using in-wheel motors, their application leads to an increase in unsprung mass, which negatively affects the ride comfort and handling stability. Under road excitation, the magnetic gap deformation of the hub motor will produce an unbalanced magnetic pull force, thus deteriorating the longitudinal and vertical dynamic performance of the vehicle [3]. Reference [4] established a dynamic model of a quarter-vehicle vibration system by using dynamic theory and state-space method. The simulation results showed that the vertical dynamic performance of the electric vehicle changes under the double excitation, and the electromagnetic force of the

*Corresponding author. E-mail address: shenyujie@ujs.edu.cn (Yujie Shen)
Executive Editor: Rui Huang

wheel motor led to a decrease in ride comfort. It also affects the grounding behavior of vehicles, causing the vertical vibration negative effect.

As a crucial component of vehicle vertical motion, the suspension is of great significance to ride comfort. Research into suspensions centers on structural design [5,6], control strategies [7,8], and actuator development [9,10]. Some scholars have researched the suppression of HMDV vertical vibration negative effect. Meng et al. [11] proposed a new electric wheel configuration with a two-stage suspension and optimized suspension parameters. Li et al. [12] developed a direct wheel drive air suspension system and proposed evaluation indexes based on vertical and longitudinal dynamic coupling mechanisms. The vertical and longitudinal characteristics under different damping coefficients and motor speed are studied, and the effectiveness of the model is verified by experiments. Liu et al. [13] presented a two-pump hydraulic control system for a two-speed power shift transmission, and simulation results show that the energy consumption of the system is significantly reduced, and the dynamic and economic performance of electric vehicles is improved. Yu et al. [14] established a hub-motor electric vehicle model with air springs. Then the quasi-infinite horizon nonlinear model predictive controller was designed to improve the longitudinal and vertical dynamic behavior.

However, the existing suspension structure is still limited to the "spring-damping" binary frame. The mass block is rarely used in the suspension because of its large volume and inconvenient installation. That leaves the suspension system without an effective inertial element. In 2002, Smith proposed the inerter [15], which is a two-end mass component. Research shows that introducing the inerter into the suspension system to form an "inerter-spring-damper" suspension structure can improve the vertical dynamic performance of the vehicle [16-24]. There are many forms of inerter such as ball-screw, rack and pinion, hydraulic, and mechatronic inerter. The mechatronic inerter is a new type of inerter device that is coupled by a mechanical inerter and motor. Wang and Chan [25] first proposed the device and optimized the electrical network structure to improve the vibration isolation performance of the suspension. According to the different mechanical transmission modes, it can be divided into single motor type, linear inerter-motor type, and rotary inerter-motor type. The first type is a special mechatronic inerter, which directly couples the motor with the mechanical vibration isolation system [26]. It simulates the impedance characteristics of the system using the output force of the motor. The linear inerter-motor type combines a linear motion type inerter with a linear motor, such as a hydraulic electric inerter [27]. The rotary inerter-motor type combines a rotary inerter with a rotary motor, such as a ball-screw mechatronic inerter in Ref. [25]. The two latter types of system output impedance consist of the impedance of the mechanical device and the simulated impedance of the motor.

The advantage of the mechatronic inerter is that the target mechanical impedance can be simulated using electrical elements in the external circuit. This allows the implementation of over-complicated purely mechanical networks to be solved. The theory of network analysis in the field of electricity can also be used to solve the vibration isolation research of mechanical systems. On the one hand, the output impedance of different structures is studied forward through network analysis. On the other hand, the physical realization of specific impedance is studied by network synthesis. Many scholars have studied the realization of the biquadratic impedance function. Bott and Duffin [28] proposed that any biquadratic positive real impedance can be realized passively by nine elements at most. Subsequently, the realization with six [29], five [30], and four [31] elements were proposed.

In order to further improve the vibration isolation effect, the higher-order impedance function has been studied. For the bicubic impedance function, a series-parallel network consisting of 13 elements is synthesized using Bott-Duffin synthesis. Reference [32] defined the concept of essential regular and implemented the impedance function using three reactive elements and four resistive elements. Hughes [33] proved that any impedance that can be realized by a series-parallel network containing at most three energy storage elements can also be realized by a series-parallel network containing at most three energy storage elements and at most four resistors.

However with the increase of the impedance function order, the number of components required also increased. To reduce the number of components, more exacting realization conditions are required. According to Pantell [34] simplification, non-series-parallel networks can achieve higher impedance functions with fewer components. References [35,36] studied biquadratic impedance and bicubic impedance using bridge networks and also gave the realization conditions of them. When using five elements to implement the impedance function, the biquadratic impedance can be realized by a bridge network containing two energy storage elements, and the bicubic impedance can be realized by a bridge network containing three energy storage elements. It is found that the increase in order seems to be related to the number of energy storage elements. Therefore, this paper selects four energy storage elements and one energy consuming element as the basic elements to analyze their impedance functions. There are two types of components in energy storage components: inductor and capacitor. For a bridge network with five components four of which are energy storage elements, the following combination modes are included: (1) 4 inductors and 1 resistor; (2) 4 capacitors and 1 resistor; (3) 3 inductors, 1 capacitor, and 1 resistor; (4)

3 capacitors, 1 inductor, and 1 resistor; (5) 2 inductors, 2 capacitors, and 1 resistor. These combination methods can form 23 different structures, and analyzing them all would be a complex and massive task. Therefore, for the convenience of research, the combination of 2 inductors, 2 capacitors, and 1 resistor is chosen for study.

In this paper, the impedance of the network structure is analyzed forward based on the bridge network, so as to avoid the complicated discussion of the realization conditions. The bridge network is coupled with a single motor to export force and improve the vibration isolation effect of HMDV suspension. The suppressing effect of different networks on the negative effect of vertical vibration of HMDV is studied. Aiming at improving vehicle grounding, the influence between the parameters of bridge network elements and suspension output response is analyzed. Then the suppression rule of the network structure on the negative effect of HMDV vertical vibration is studied. Firstly, the quarter HMDV model equipped with a switched reluctance motor (SRM) is built in Sect. 2. Then in Sect. 3, the impedance functions of the bridge network are solved by using the topological formulas. The element parameters in the network are optimized by using the Pattern Search algorithm. Moreover, in Sect. 4, the improvement effect of different structures of bridge network on HMDV vertical vibration negative effect is analyzed, and the influence between parameter changes and suspension output response is studied. Finally, some conclusions are drawn in Sect. 5.

2. HMDV mechatronic suspension model

2.1 SRM model

SRM has the characteristics of simple structure, large torque and small current at starting and low speed. It has high output and high efficiency in a wide speed and power range. It also has the advantages of good fault tolerance so it has a wide range of applications. In this paper, the external rotor 8/6 pole four-phase SRM is selected as the research object. The structure of the SRM is shown in Fig. 1 [37].

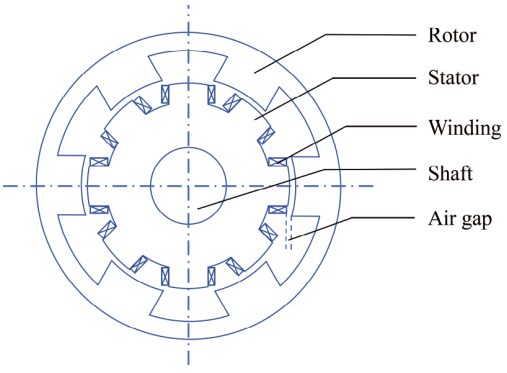

Figure 1 Structure of external rotor 8/6 pole four-phase SRM.

Radial electromagnetic force is the main source of noise and vibration of the SRM. Theoretically, the radial electromagnetic force is equal in magnitude and opposite in direction, so its resultant force is 0. However, because the air gap of the motor changes due to road excitation, the radial electromagnetic force is not really 0, and the motor eccentricity is defined as

$$\varepsilon = \frac{h_e}{g_m}, \tag{1}$$

where h_e is the absolute eccentricity of the motor, and g_m is the air gap of the motor.

Therefore, the radial electromagnetic force F_{rm} between the fixed rotor of the motor is

$$F_{rm} = -\frac{1}{2}i^2\frac{L_j(\theta, i_j)}{g_m(m)}, \tag{2}$$

where $L_j(\theta, i_j)$ is the inductance expressed in Fourier series [38-40] of the phase j, which corresponds to the rotor angular position and the winding current. Therefore, the unbalanced radial force of the phase j:

$$F_{rj} = F_{rm} - F_{rn} = \frac{1}{2}i^2\frac{L_j(\theta, i_j)}{g_m(n)} - \frac{1}{2}i^2\frac{L_j(\theta+\pi, i_j)}{g_m(m)}, \tag{3}$$

Where m and n are the pole number of stator in the opposite direction, $g_m(n) = (1-\varepsilon)g_m$, $g_m(m) = (1+\varepsilon)g_m$ and $|m-n| = 4$.

For the HMDV system established in this paper, the vertical component of the unbalanced radial force is the main influencing factor. The total vertical electromagnetic force is the sum of the 4 phase electromagnetic forces, which is

$$F_z = \sum_{k=1}^{4} F_{rjz} = \sum_{k=1}^{4} F_{rj}\cos\theta\frac{-b \pm \sqrt{b^2-4ac}}{2a}. \tag{4}$$

2.2 Mechatronic suspension model

The 2-DOF vehicle suspension model considering the vertical vibration of sprung and unsprung mass is often used to study the vertical dynamic performance of vehicles. In this paper, a quarter vehicle dynamic model is selected as the research object, and the model is shown in Fig. 2. In the suspension part, the linear motor is used to equate the electrical impedance to the mechanical impedance. When the sprung mass moves relative to the stator, both ends of the motor also move and generate current. Then the current flows through the circuit at the external end of the motor to achieve the effect of equating the electrical network impedance to the mechanical impedance. This makes the original complex mechanical structure can be realized through the electrical network, which brings great convenience to the practical application. Through the design and analysis of the circuit structure, the influence of different structures on the vertical dynamic performance of the vehicle can be studied.

In Fig. 2, m_s is the sprung mass, m_{us} is the mass of the stator of the wheel hub motor, and m_{ur} is the mass of the rotor and tire. k_s is the suspension spring stiffness, k_m is the equivalent stiffness of the motor, and K_t is the stiffness of the tire. z_s is the vertical displacement of sprung mass, z_{us} is the vertical displacement of stator and shaft, z_{ur} is the vertical displacement of rotor and tire, and z_r is the road excitation. F_{EM} is the electromagnetic force generated by the linear motor, V is the end voltage generated by the linear motor, Z_{Si} (i = 1, 2, 3, 4, 5) is the electrical element in the bridge network circuit outside the motor, including 2 inductors, 2 capacitors, and 1 resistor, F_z is the vertical unbalance force caused by the wheel motor. The internal inductance and resistance of linear motor are ignored in modeling. According to Newton's second law, the Laplace transform of the dynamic equation is shown as Eq. (5).

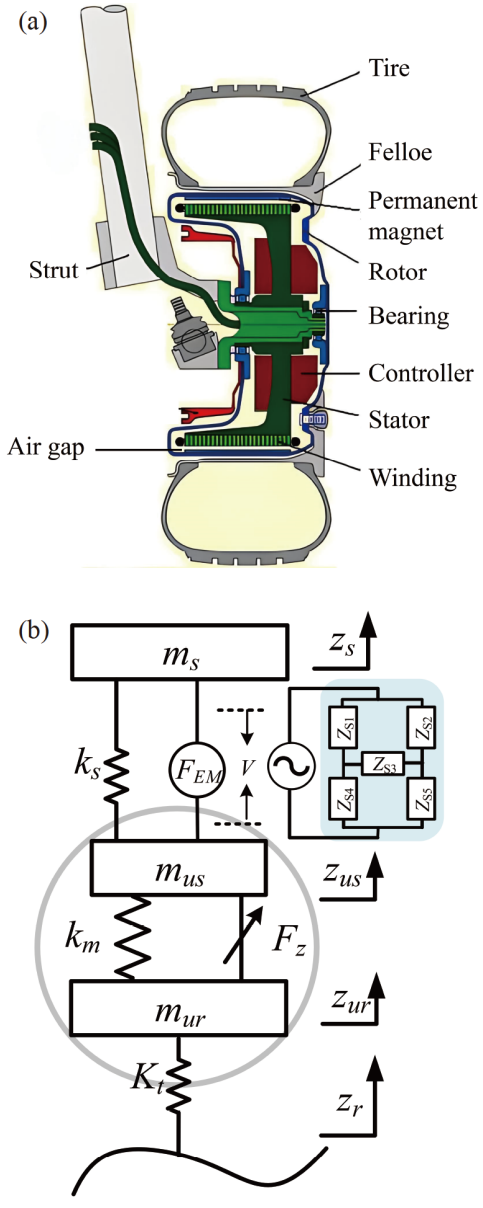

Figure 2 Vehicle structure of HMDV: (a) the typical structure of HMDV, and (b) quarter-vehicle model.

$$\begin{cases} m_s s^2 Z_s + k_s(Z_s - Z_{us}) + F_{EM} = 0, \\ m_{us} s^2 Z_{us} + k_m(Z_{us} - Z_{ur}) + F_z - k_s(Z_s - Z_{us}) - F_{EM} = 0, \\ m_{ur} s^2 Z_{ur} + K_t(Z_{ur} - Z_r) - k_m(Z_{us} - Z_{ur}) - F_z = 0. \end{cases} \tag{5}$$

The calculation method of F_{EM} is given by Eq. (6), where I is the current flowing through the external circuit of the motor, k_t is the thrust coefficient of the linear motor, and k_e is the electromotive force coefficient of the linear motor.

$$\begin{cases} V = k_e s(Z_s - Z_{us}) = IZ_e(s), \\ F_{EM} = k_t I. \end{cases} \tag{6}$$

Then F_{EM} is shown in Eq. (7):

$$F_{EM} = \frac{k_e k_t}{Z_e(s)} s(Z_s - Z_{us}), \tag{7}$$

where Z_s, Z_{us}, and Z_{ur} are the Laplace transform of the displacement, respectively, $Z_e(s)$ is the impedance of the external circuit, and s is the Laplace variable.

Conventional suspension consists of springs and dampers. Vehicle suspensions are tested and adjusted during the design process to ensure ride comfort and handling stability. To compare the dynamic performance of vehicles after the application of the bridge network, this paper takes a mature passenger car with conventional suspension as the comparison object, and the parameters of a quarter vehicle model are shown in Table 1.

3. Bridge network and parameter optimization

3.1 Impedance function of the bridge network

Chen et al. [35] used a five-element structure with two energy storage elements to establish biquadratic functions. Wang and Chen [36] gave 11 kinds of bridge networks with three energy storage elements to realize bicubic impedance. Therefore, this paper will establish a bridge network structure with four energy storage components, and the impedance function of the bridge network will be analyzed

Table 1 Parameters of the quarter vehicle model

Parameter	Value
Sprung mass m_s (kg)	320
Motor stator mass m_{us} (kg)	35
Motor rotor and unsprung mass m_{ur} (kg)	40
Suspension spring stiffness k_s (N/m)	22000
Equivalent motor stiffness k_m (N/m)	3850000
Equivalent tire stiffness K_t (N/m)	190000
Thrust coefficient of linear motor k_t (N/A)	0.99
Electromotive force coefficient of linear motor k_e (V·m/s)	0.99

forwardly. From the component structure, the analysis avoids the complicated discussion of the conditions required for the synthesis of the positive real network. To facilitate the study, this paper selects 2 inductors, 2 capacitors, and 1 resistor to build a bridge network, and enumerates them to obtain the nine structures shown in Fig. 3.

The impedance functions of the above nine structures are calculated using the topological formula of the network function [41]. This section only shows the impedance of the three structures Z_1, Z_3, and Z_7. To facilitate the calculation of linear motor thrust, the reciprocal expressions of the impedance function are shown in Eqs. (8)-(13). The impedance of other structures is in Appendix.

$$\frac{1}{Z_1(s)}=\frac{A_1s^4+B_1s^3+C_1s^2+D_1s+E_1}{F_1s^4+G_1s^3+H_1s^2+I_1s+J_1}, \tag{8}$$

$$\begin{cases} A_1=0,\\ B_1=C_1C_2R(L_1+L_2),\\ C_1=(L_1+L_2)(C_1+C_2),\\ D_1=R(C_1+C_2),\\ E_1=0,\\ F_1=RL_1L_2C_1C_2,\\ G_1=L_1L_2(C_1+C_2),\\ H_1=R(L_1C_1+L_2C_2),\\ I_1=(L_1+L_2),\\ J_1=R, \end{cases} \tag{9}$$

$$\frac{1}{Z_3(s)}=\frac{A_3s^4+B_3s^3+C_3s^2+D_3s+E_3}{F_3s^4+G_3s^3+H_3s^2+I_3s+J_3}, \tag{10}$$

$$\begin{cases} A_3=L_1L_2C_1C_2,\\ B_3=RC_1C_2(L_1+L_2),\\ C_3=L_1C_1+L_2C_2,\\ D_3=R(C_1+C_2),\\ E_3=1,\\ F_3=0,\\ G_3=L_1L_2(C_1+C_2),\\ H_3=R(L_1+L_2)(C_1+C_2),\\ I_3=(L_1+L_2),\\ J_3=0, \end{cases} \tag{11}$$

$$\frac{1}{Z_7(s)}=\frac{A_7s^4+B_7s^3+C_7s^2+D_7s+E_7}{F_7s^4+G_7s^3+H_7s^2+I_7s+J_7}, \tag{12}$$

$$\begin{cases} A_7=L_1L_2C_1C_2,\\ B_7=RC_1C_2(L_1+L_2),\\ C_7=L_1C_2+L_2(C_1+C_2),\\ D_7=RC_1,\\ E_7=1,\\ F_7=RL_1L_2C_1C_2,\\ G_7=L_1L_2C_1,\\ H_7=RL_1(C_1+C_2)+RL_2C_2,\\ I_7=(L_1+L_2),\\ J_7=R. \end{cases} \tag{13}$$

After analysis, it is found that the impedance functions of Z_2, Z_4, Z_5, Z_6, and Z_7 are all of the strict biquartic types, that is, the highest order of numerator and denominator are 4. The impedance functions of other structures are non-strict

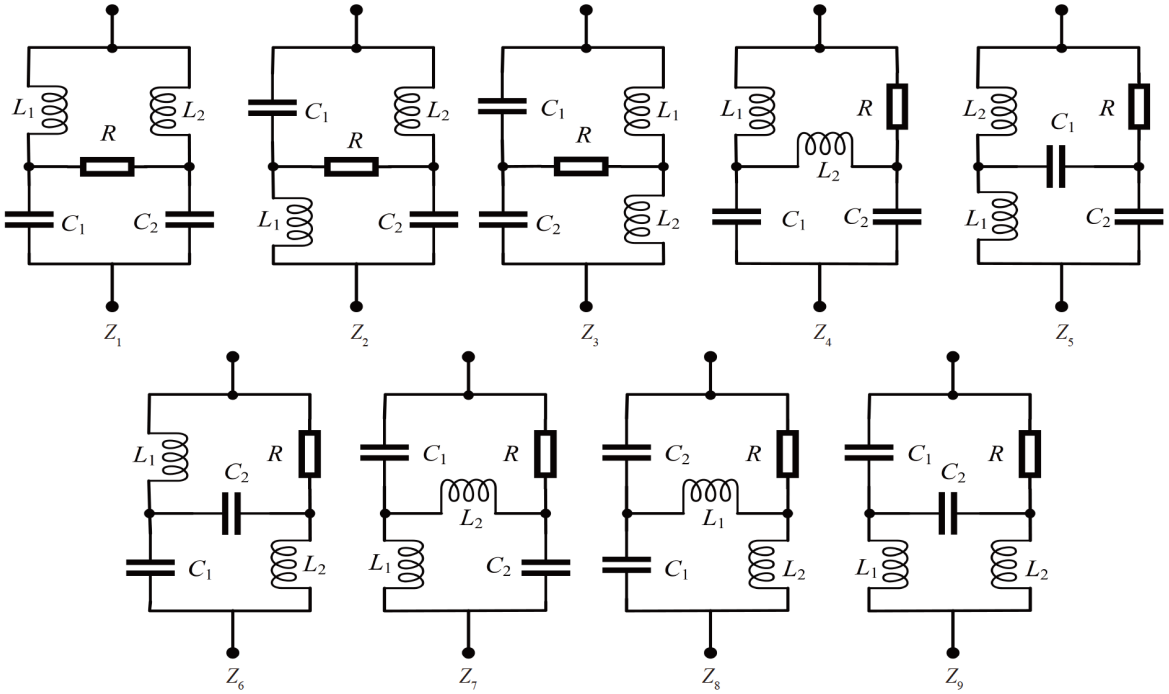

Figure 3 Bridge network structure with 2 inductors, 2 capacitors, and 1 resistor.

biquartic functions. The highest order numerator in Z_1 and Z_9 is 3, and the highest order denominator is 4, which means A_1 and A_9 are equal to 0, the impedance functions of Z_3 and Z_8 are just the opposite, and F_3 and F_8 are equal to 0.

3.2 Dynamic performance optimization

In the suspension optimization process, assuming that the vehicle is driving at a speed of u = 20 m/s on a C-class road, the input displacement of road roughness can be expressed as follows:

$$\dot{z}_r(t) = -0.111\left[uz_r(t) + 40\sqrt{G_q(n_0)u}\,w(t)\right], \tag{14}$$

where $z_r(t)$ is the vertical input displacement caused by the roughness of the model road surface, $G_q(n_0)$ is the road roughness coefficient, the value is 2.56×10^{-4} m^3,and $w(t)$ represents integral white noise.

3.2.1 Optimization algorithm

Pattern search algorithm is a general algorithm to solve the optimal value of the function. It does not need to use the derivative of the objective optimization function in the search process, so it can effectively solve the in-differentiable function and the complicated function optimization problem. The detailed steps of the pattern search method are shown in Fig. 4.

Each iteration of this algorithm alternates between axial and pattern movements. The purpose of axial movement is to detect the favorable direction of descent, while the purpose of pattern movement is to accelerate along the favorable direction. Axial movement is an exploratory search movement that starts from a point y and searches for probing movement with step size δ_k along the axis e_j ($j = 1, 2, \cdots, n$) in turn. The probing movement along the axis is as follows:

(1) Positive axis detection

If $f\left(y+\delta_k e_j\right) < f(y)$, the detection is successful, take $y = y+\delta_k e_j$; Otherwise, the detection will fail and the negative axis detection will be performed again.

(2) Negative axis detection

If $f\left(y-\delta_k e_j\right) < f(y)$, the detection is successful, take $y = y-\delta_k e_j$; Otherwise, the detection fails and y remains unchanged.

The point obtained after each probe movement is used as the starting point for the next probe movement. After the n steps of detecting movement, the point at which the objective function value decreases can generally be obtained, thus an axial movement is completed. The starting point of each axial movement is called the reference point.

Let x_{k+1} be the point obtained by a single axial movement with point x_k as the reference point. If $f(x_{k+1}) < f(x_k)$, then start from point x_{k+1} and move in a pattern with a step size of αd_k along the acceleration direction $d_k = x_{k+1} - x_k$ to obtain a new reference point. Then, start from the new reference point y and continue to move axially with the same step size of δ_k.

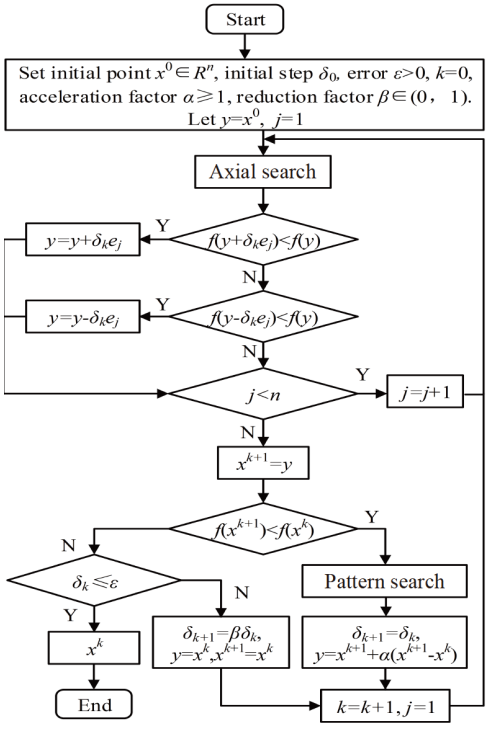

Figure 4 Algorithm flow chart.

3.2.2 Optimization objectives and constraints

The negative vertical vibration effect of HMDV is caused by the significant increase of sprung mass, which leads to the deterioration of dynamic tire load. In order to improve its tire grounding, this paper selects the root-mean-square (RMS) value of the dynamic tire load as the optimization objective and establishes the objective function, which is given by Eq. (15). The optimization object is the element parameters in nine kinds of electrical network structures. Then the structure values under the optimal dynamic response can be obtained.

$$\min J = \frac{DTL_i}{DTL_{\text{pas}}}, \tag{15}$$

$$q = [C_1, C_2, L_1, L_2, R], \tag{16}$$

where DTL_i represents the RMS value of dynamic tire load with bridge network suspension structure, DTL_{pas} represents the RMS value of dynamic tire load of conventional suspension, J represents the ratio of them, and q represents the set of electrical network element parameters to be optimized.

To obtain electrical network parameters with better per-

formance, this paper establishes certain constraint conditions to ensure that the optimized performance is better than that of the traditional structure. The DTL_i of the bridge network suspension structure should be smaller than the DTL_{pas} of the conventional suspension. The RMS values of body acceleration BA_i and suspension working space SWS_i of bridge network suspension are smaller than those of conventional suspension. At the same time, considering the rationality of the components, the optimization constraints are set as follows:

$$s.t.\begin{cases} BA_i < BA_{\text{pas}}, \\ SWS_i < SWS_{\text{pas}}, \\ DTL_i < DTL_{\text{pas}}, \\ 0 < L_{1,2} < 800\ \text{mH}, \\ 0 < C_{1,2} < 800\ \text{mF}, \\ 0 < R < 1000\ \Omega. \end{cases} \tag{17}$$

3.3 Optimization results and time domain response

After several optimizations, the optimal parameters of the suspension structure were obtained, as shown in Table 2. The parameters from Tables 1 and 2 were combined and substituted into the model to analyze the suspension's output response, as shown in Table 3.

In Table 3, Z_0 represents the conventional suspension structure, and the percentage in parentheses represents the comparison results between this indicator and the conventional suspension. The upward arrow indicates that the indicator has deteriorated, while the downward arrow indicates that the indicator has been optimized compared to conventional suspension. As shown in Table 3, after optimizing all structures, the RMS value of dynamic tire load is improved, and the RMS values of suspension working space and body acceleration are also reduced. It is worth noting that the impedance functions of Z_1, Z_3, Z_8, and Z_9 are not strictly biquartic, which also makes the performance improvement of these structures for HMDV less obvious than the others. The body acceleration of Z_3 and Z_8 even slightly deteriorated. Among several structures with strict biquartic impedance function, Z_7 has the best improvement effect. Its time-domain response is shown in Fig. 5.

Compared with conventional suspension, its RMS value of dynamic tire load is reduced by 10.76%, and the RMS value of suspension working space is reduced by 18.10%. Moreover, the body acceleration is also improved by 1.45%. The application of this structure can improve the handling stability of the vehicle based on ensuring ride comfort. Then suppress the negative vertical vibration effect of HMDV.

To further verify the effectiveness of the established mechatronic suspension, the parameters of the Z_7 structure in Table 2 and different road inputs were used to analyze its time domain response. According to Eq. (14), the road displacement input is not only related to road roughness but also to the vehicle's driving speed. Therefore, by changing

Table 2 Results of optimization design

Structure	Parameters				
	C_1 (mF)	C_2 (mF)	R (Ω)	L_1 (mH)	L_2 (mH)
Z_1	397.2	278.9	706	1.48	1.37
Z_2	611.6	361.7	670	1.28	2.39
Z_3	1.5	0.08	950	3.5	99.8
Z_4	429.8	397.4	701	1.8	588.7
Z_5	451.5	354.1	734	91.2	1.3
Z_6	677.1	336.7	763	1	585.8
Z_7	193.1	644.7	615	1	1
Z_8	1.25	267.6	893	3.2	180.4
Z_9	201.6	522	831	1	2.6

Table 3 Performance indexes of different suspension

Structure	RMS of body acceleration (m/s^2)	RMS of suspension working space (m)	RMS of dynamic tire load (N)
Z_0	1.3178	0.0139	1228.16
Z_1	1.2931 (1.88%↓)	0.0124 (10.31%↓)	1118.64 (8.92%↓)
Z_2	1.2968 (1.59%↓)	0.0122 (12.03%↓)	1135.66 (7.53%↓)
Z_3	1.3269 (0.69%↑)	0.0138 (0.76%↓)	1123.81 (8.50%↓)
Z_4	1.2943 (1.78%↓)	0.0120 (13.88%↓)	1127.85 (8.17%↓)
Z_5	1.2810 (2.79%↓)	0.0119 (14.21%↓)	1136.44 (7.47%↓)
Z_6	1.2835 (2.60%↓)	0.0120 (13.19%↓)	1145.77 (6.71%↓)
Z_7	1.2986 (1.45%↓)	0.0114 (18.10%↓)	1096.06 (10.76%↓)
Z_8	1.3341 (1.23%↑)	0.0136 (2.05%↓)	1116.68 (9.08%↓)
Z_9	1.2916 (1.99%↓)	0.0129 (6.73%↓)	1120.78 (8.74%↓)

one of the values within a certain range, a series of different road input conditions can be obtained. In this article, the road roughness is set as a constant value, and the vehicle speed u is changed to 10 m/s, 20 m/s, and 30 m/s. The time domain response at 20 m/s is shown in Fig. 5, the time domain response at 10 m/s is shown in Fig. 6(a)-(c), and the time domain response at 30 m/s is shown in Fig. 6(d)-(f). The data in Tables 4 and 5 are the RMS values of the time domain response of performance indexes at different speeds and their improvement effects compared to conventional suspension.

From Fig. 6, Tables 4 and 5, it can be seen that the Z_7 structure has also achieved significant performance improvements at different vehicle speeds. When the vehicle travels at a speed of 10 m/s, using a suspension with the Z_7 structure can reduce the RMS value of dynamic tire load by 10.66%, and the body acceleration can also be maintained at a level close to that of conventional suspension. Although the improvement effect of the Z_7 structure on three indexes is slightly worse than 20 m/s at 10 m/s, it significantly reduces the RMS value of dynamic tire load under the same conditions, effectively improving tire grounding. When driving at a speed of 30 m/s, there may be a slight deterioration of less than 1% in vehicle body acceleration, but it is still within an acceptable range. The RMS values of suspension working space and dynamic tire load were reduced by 18.22% and 10.79%, respectively. Overall, the Z_7 structure can also suppress the negative vertical vibration effect of HMDV at this speed, and improve tire grounding and handling stability. Therefore, the suspension with Z_7 is selected as the research structure, and its dynamic characteristics are analyzed in the next section.

4. Dynamic performance analysis

4.1 Frequency domain analysis

The Z_7 is selected as the research object, and the suspension structure parameters are set according to the optimization parameters in Table 2. The Z_1, Z_3, and conventional suspension were compared. The gain of body acceleration gain, suspension working space, and dynamic tire load of the four suspensions in the frequency domain are shown in Fig. 7.

As can be seen from Fig. 7, the gain of dynamic tire load with bridge network in low frequency band and high frequency band is smaller than that of conventional suspension.

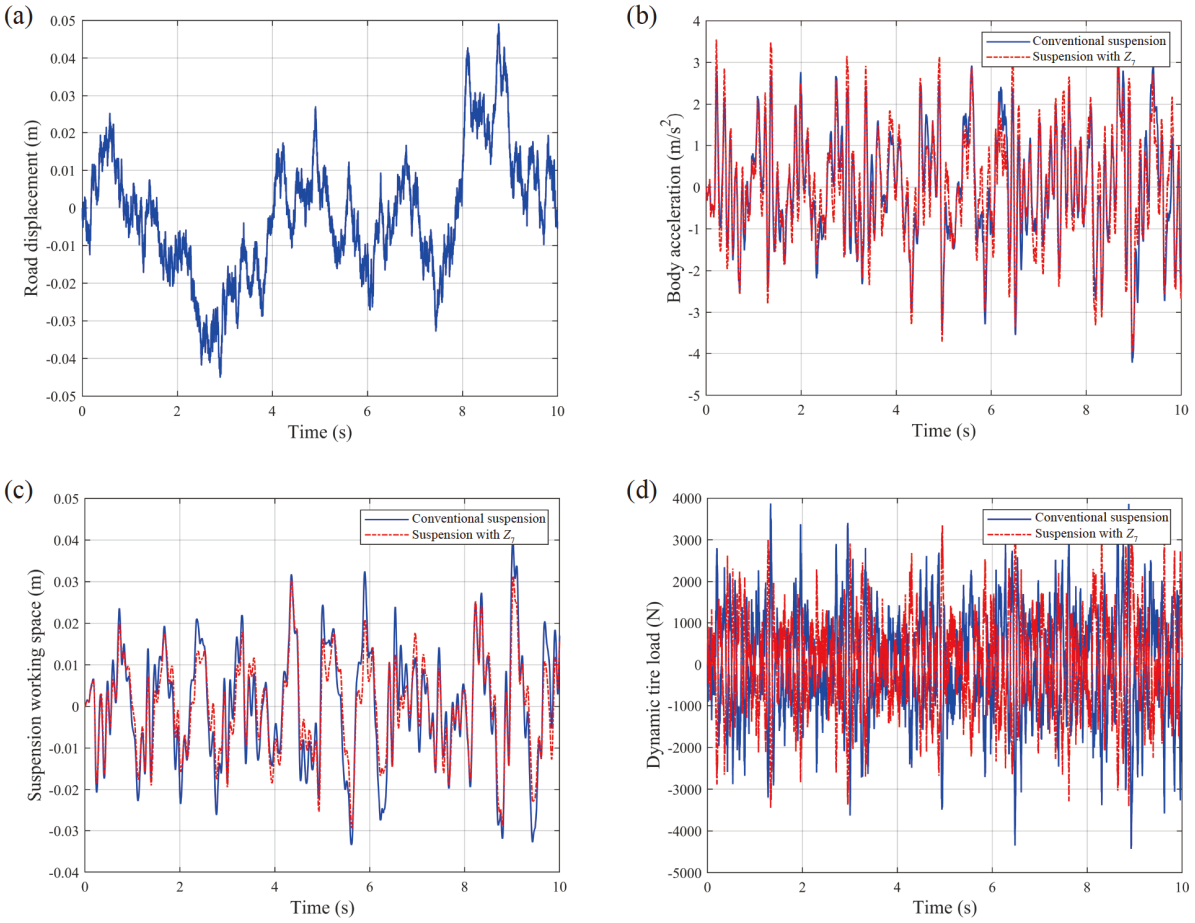

Figure 5 Road displacement and time domain comparison of suspension performance at 20 m/s: (a) road displacement, (b) body acceleration, (c) suspension working space, and (d) dynamic tire load.

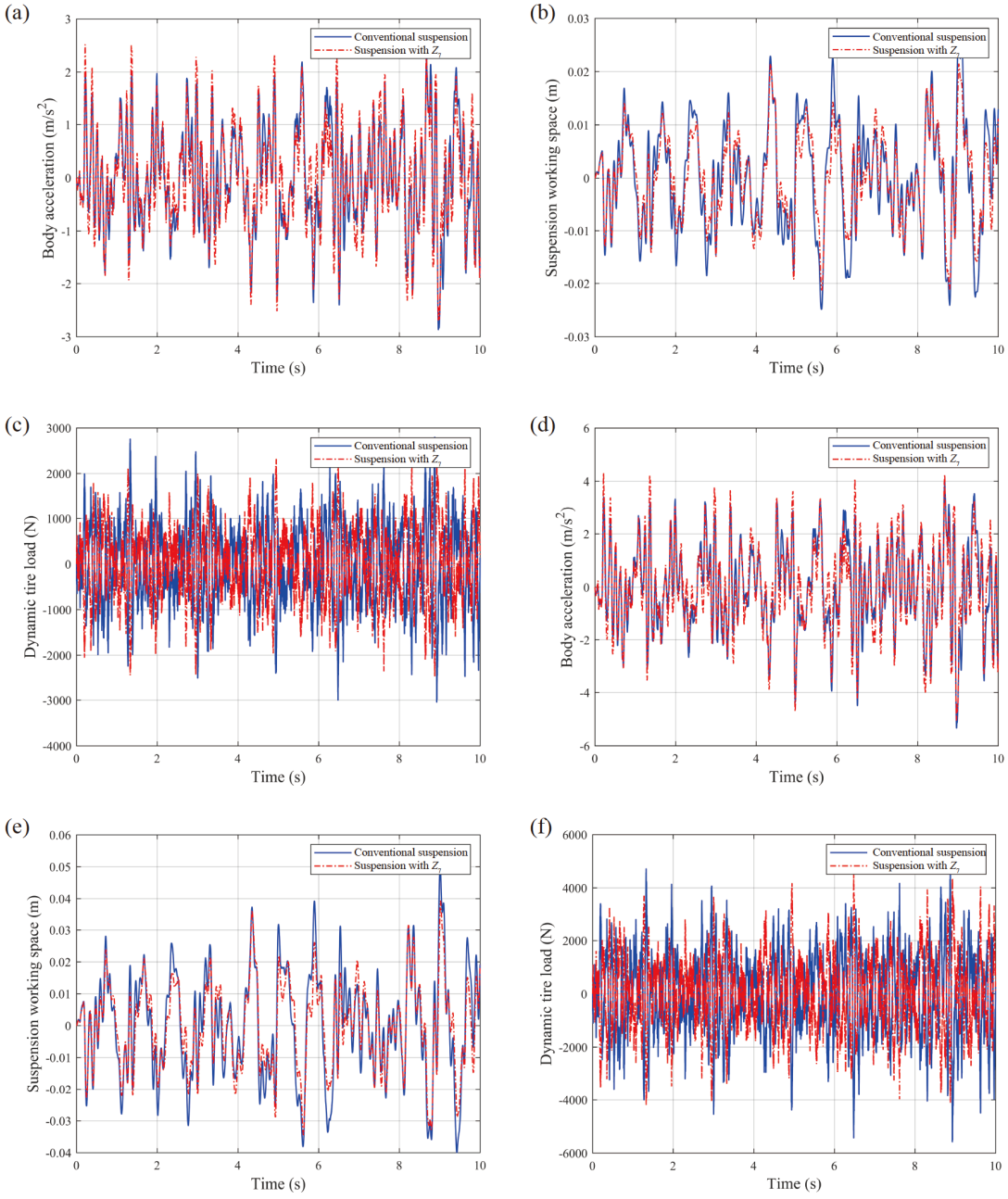

Figure 6 Road displacement and time domain comparison of suspension performance: (a) body acceleration at 10 m/s, (b) suspension working space at 10 m/s, (c) dynamic tire load at 10 m/s, (d) body acceleration at 30 m/s, (e) suspension working space at 30 m/s, and (f) dynamic tire load at 30 m/s.

Table 4 Performance indexes at 10 m/s

	Conventional suspension	Suspension with Z_7	Improvement
RMS of body acceleration (m/s^2)	0.9424	0.9365	0.63%
RMS of suspension working space (m)	0.0100	0.0083	17.88%
RMS of dynamic tire load (N)	867.34	774.90	10.66%

Table 5 Performance indexes at 30 m/s

	Conventional suspension	Suspension with Z_7	Improvement
RMS of body acceleration (m/s^2)	1.5866	1.6011	−0.91%
RMS of suspension working space (m)	0.0165	0.0135	18.22%
RMS of dynamic tire load (N)	1503.66	1341.40	10.79%

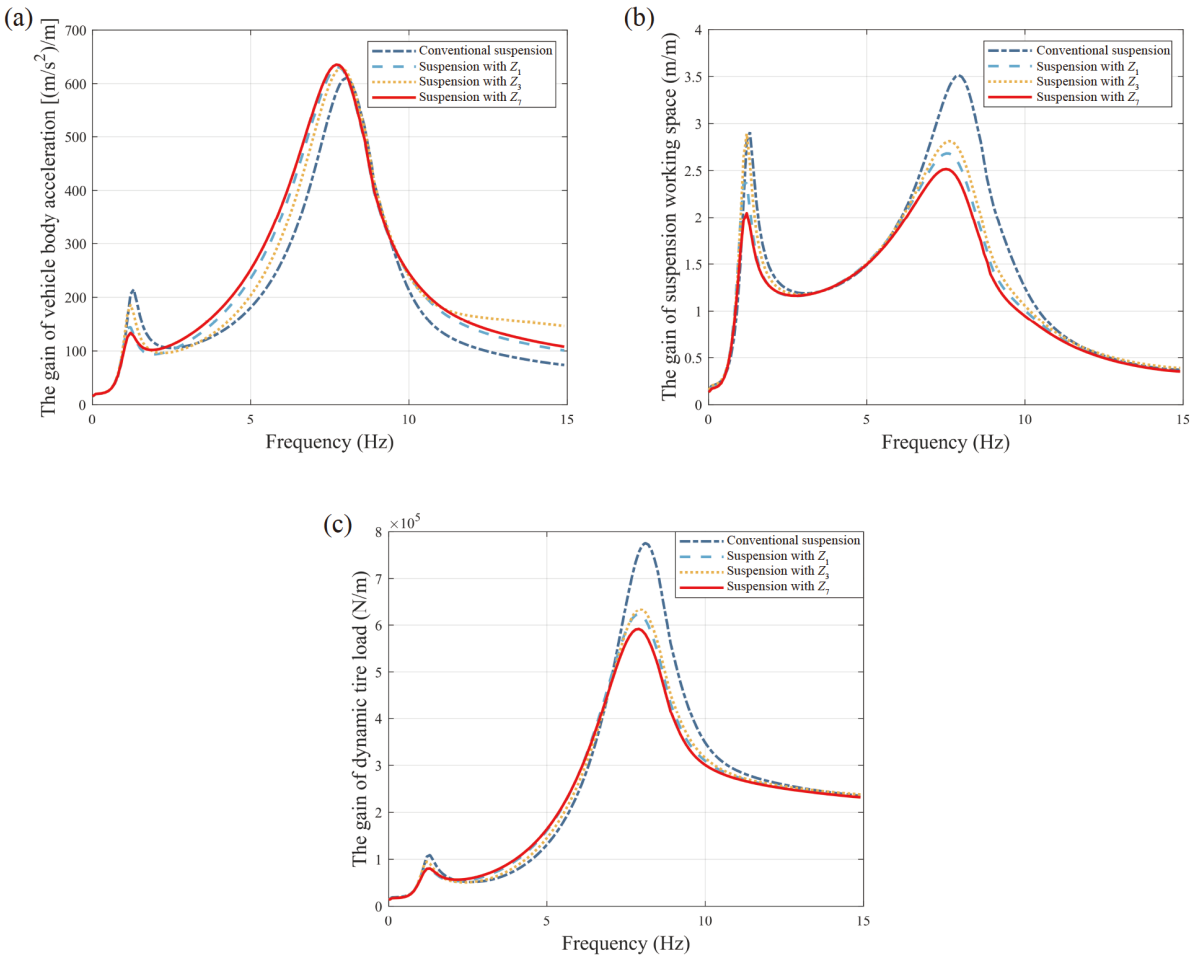

Figure 7 Comparison of frequency domain gain of four types of suspension: (a) the gain of vehicle body acceleration, (b) the gain of suspension working space, (c) the gain of dynamic tire load.

It indicates that the equivalent mechanical impedance of the bridge network structure can suppress vehicle vibration. It also points out that the suppression effect is better in the low frequency band and high frequency band, and the Z_7 structure has the best effect. Although slightly higher than the conventional suspension between 2-7 Hz, the overall effect is still better than the conventional suspension. The advantage of the bridge network is more remarkable in the gain of suspension working space. As this paper focuses on the negative vertical vibration effect of HMDV, the improvement of dynamic tire load is quite obvious. In terms of body acceleration, low-frequency vibration can be suppressed. But in the middle and high frequency bands, it is almost the same as that of conventional suspension and even has a slight worsening trend.

On the one hand, it is because of the selection of optimization focus. On the other hand, it is the increase of energy conversion process. Conventional suspension converts kinetic energy into spring potential energy and the internal energy of the oil in the damper. The linear motor, as an energy conversion device, converts kinetic energy into electric energy first. Then consumes energy in the form of resistance heating. Under the high frequency excitation, the energy input speed is accelerated, and the energy dissipation component fails to totally absorb the input energy in time. Part of the energy is transferred to the sprung mass, increasing the gain about body acceleration. But in general, the use of bridge network structure to equivalent mechanical impedance still has the advantages of simple, no complex mechanical components, and can effectively inhibit vehicle vibration.

4.2 Discussion on frequency domain characteristics of three structures

In vehicle vibration analysis, the damping ratio is commonly used to describe the amplitude-frequency characteristics of vibration response to input, which is defined as Eq. (18). Vehicles with lower damping ratios can achieve high comfort while achieving better tire adhesion performance requires a higher damping ratio. Sports cars typically have a large damper and harder tire stiffness, while luxury cars typically have a small damper and softer springs. The force between the two ends of a linear motor is related to the

relative velocity between the sprung mass and the unsprung mass, which is similar to the working mode of a damper. Compared with the concept of "damping ratio", the damping coefficient in the damping ratio is replaced by the impedance of the electrical network of the outer end of the linear motor. And the ratio obtained can be considered an "equivalent damping ratio", as shown in Eq. (19).

$$\zeta = \frac{C}{2\sqrt{k_s m_s}}, \tag{18}$$

$$\zeta_e = \frac{k_e k_t / Z_e(s)}{2\sqrt{k_s m_s}}. \tag{19}$$

Let $T(s) = k_e k_t / Z_e(s)$, then the $T(s)$ of three structures can be expressed as Eq. (20).

$$T_i(s) = k_e k_t \frac{F_i s^4 + G_i s^3 + H_i s^2 + I_i s + J_i}{A_i s^4 + B_i s^3 + C_i s^2 + D_i s + E_i}, (i = 1, 3, 7). \tag{20}$$

Let $s = j\omega$, then $T(s)$ can be written as Eq. (21). $T(s)$ contains the impedance function of the external electrical network, which has both real and imaginary parts. In order to compare the equivalent damping ratio, its modulus is taken for calculation as Eq. (22).

$$T_i(j\omega) = k_e k_t \frac{\left(F_i\omega^4 - H_i\omega^2 + J_i\right) + \left(I_i\omega - G_i\omega^3\right)j}{\left(A_i\omega^4 - C_i\omega^2 + E_i\right) + \left(D_i\omega - B_i\omega^3\right)j}, \tag{21}$$

$(i = 1, 3, 7)$,

$$\left|T_i(j\omega)\right| = k_e k_t \sqrt{\frac{F_i^2\omega^8 + \left(G_i^2 - 2F_iH_i\right)\omega^6 + \left(H_i^2 + 2F_iJ_i - 2I_iG_i\right)\omega^4 + \left(I_i^2 - 2H_iJ_i\right)\omega^2 + J_i^2}{A_i^2\omega^8 + \left(B_i^2 - 2A_iC_i\right)\omega^6 + \left(C_i^2 + 2A_iE_i - 2B_iD_i\right)\omega^4 + \left(D_i^2 - 2C_iE_i\right)\omega^2 + E_i^2}}, (i = 1, 3, 7). \tag{22}$$

The equivalent damping ratio is shown in Eq. (23).

$$\zeta_{ei} = \frac{\left|T_i(j\omega)\right|}{2\sqrt{k_s m_s}}, (i = 1, 3, 7). \tag{23}$$

Unlike the fixed value of the damping ratio, the equivalent damping ratio of the bridge network structure is a function of frequency. Let $\omega = 2\pi f$ then analyze the equivalent damping ratio of the suspension with Z_1, Z_3, and Z_7, and the results are shown in Fig. 8.

According to Fig. 8, the equivalent damping ratio of the suspension with Z_7 can stabilize and remain around 0.2 after 2 Hz. The suspension with Z_1 reaches its maximum equivalent damping ratio around 0.9 Hz, but then rapidly decreases and tends towards 0.17. The equivalent damping ratio of the suspension with Z_3 rapidly reaches 0.13 at 0.1 Hz and continues to increase thereafter. Although its equivalent damping ratio exceeds that of the Z_7 at 12 Hz, it is lower than that of the Z_7 before 12 Hz. The purpose of this paper is to reduce the dynamic tire load of HMDV to improve the negative effects of vertical vibration. Compared to the other two types of suspension, the Z_7 can achieve a higher equivalent damping ratio, which is beneficial for improving tire adhesion and reducing dynamic tire load. Therefore, the suspension with Z_7 can reduce the vibration peak of dynamic tire load at low and high frequencies, but it will bring a slight deterioration in comfort, which is consistent with the analysis conclusion of the damping ratio.

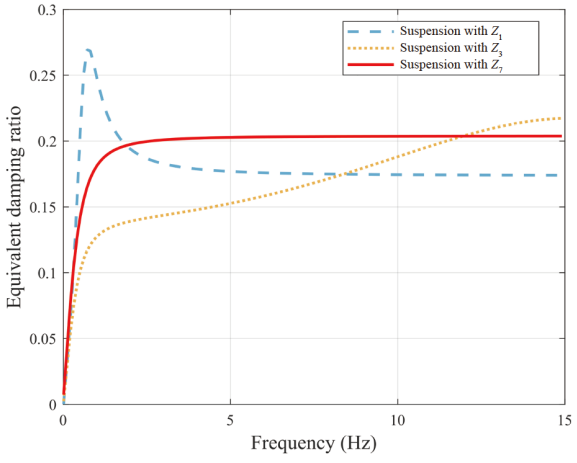

Figure 8 Comparison of the equivalent damping ratio of three types of suspension.

4.3 Influence of interaction between components on suspension performance

Because the bridge network structure is different from the series-parallel network structure, there are some influence relationships between the component parameters. Therefore, the Z_7 structure is taken as the research object. The vertical output response of the suspension is analyzed in the time domain when the energy storage elements and the energy dissipation elements change parameters. Then the interaction law between the elements is studied. L_1, L_2, C_1, and C_2 are energy storage elements, and R is energy dissipation elements. Table 6 shows the parameter ranges of circuit components in the Z_7 structure. Figures 9-12 show the analysis results.

Figure 9(a)-(c) shows the influence of capacitors C_1 and C_2 on suspension performance, and the other pictures show

Table 6 Value ranges of structural parameters

Parameter	Value range
Inductor L_1 (mH)	0.5-1.5
Inductor L_2 (mH)	0.5-1.5
Capacitor C_1 (mF)	96.55-289.65
Capacitor C_2 (mF)	322.35-967.05
Resistor R (Ω)	307.5-922.5

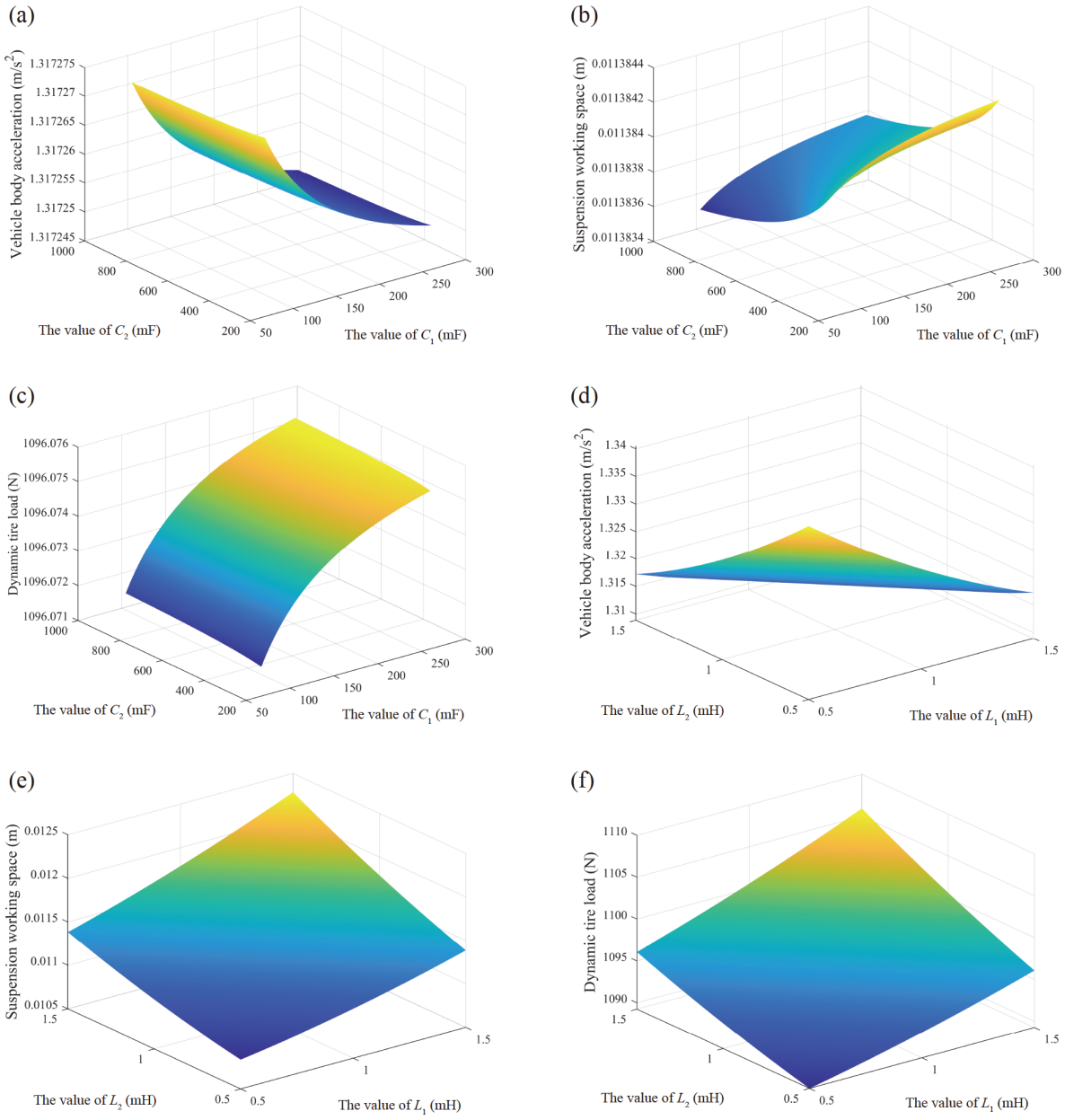

Figure 9 Influence of parameter changes of the same type of energy storage components on suspension performance: (a) effect of C_1 and C_2 variation on body acceleration, (b) effect of C_1 and C_2 variation on suspension working space, (c) effect of C_1 and C_2 variation on dynamic tire load, (d) effect of L_1 and L_2 variation on body acceleration, (e) effect of L_1 and L_2 variation on suspension working space, (f) effect of L_1 and L_2 variation on dynamic tire load.

the influence of inductors L_1 and L_2 on suspension performance. It can be seen that the combination of capacitors has a low influence on suspension performance, and the RMS values of body acceleration, suspension working space, and dynamic tire load change little. The combination of inductors has a certain influence on the suspension performance. When the two inductors are set to smaller values, the RMS value of the dynamic tire load and the suspension working space can be reduced. The handling stability and grounding of HMDV can be improved. However the RMS value of the body acceleration will be increased, and the ride comfort will be worsened. Therefore, appropriate values should be selected based on actual needs. To study the interaction between different types of energy storage elements and analyze the influence of capacitor and inductor elements on suspension performance, the combination relationship of C_1-L_1 and C_2-L_1 are taken as examples. The analysis results are shown in Fig. 10.

Figure 10 shows the influence of C_1 and L_1 on suspension performance on (a)-(c), and the influence of C_2 and L_1 on suspension performance on (d)-(f). As can be seen from Fig. 9, the RMS value of body acceleration decreases with the increase of C_1 or C_2 and remains unchanged with the increase of L_1. The RMS values of suspension working space

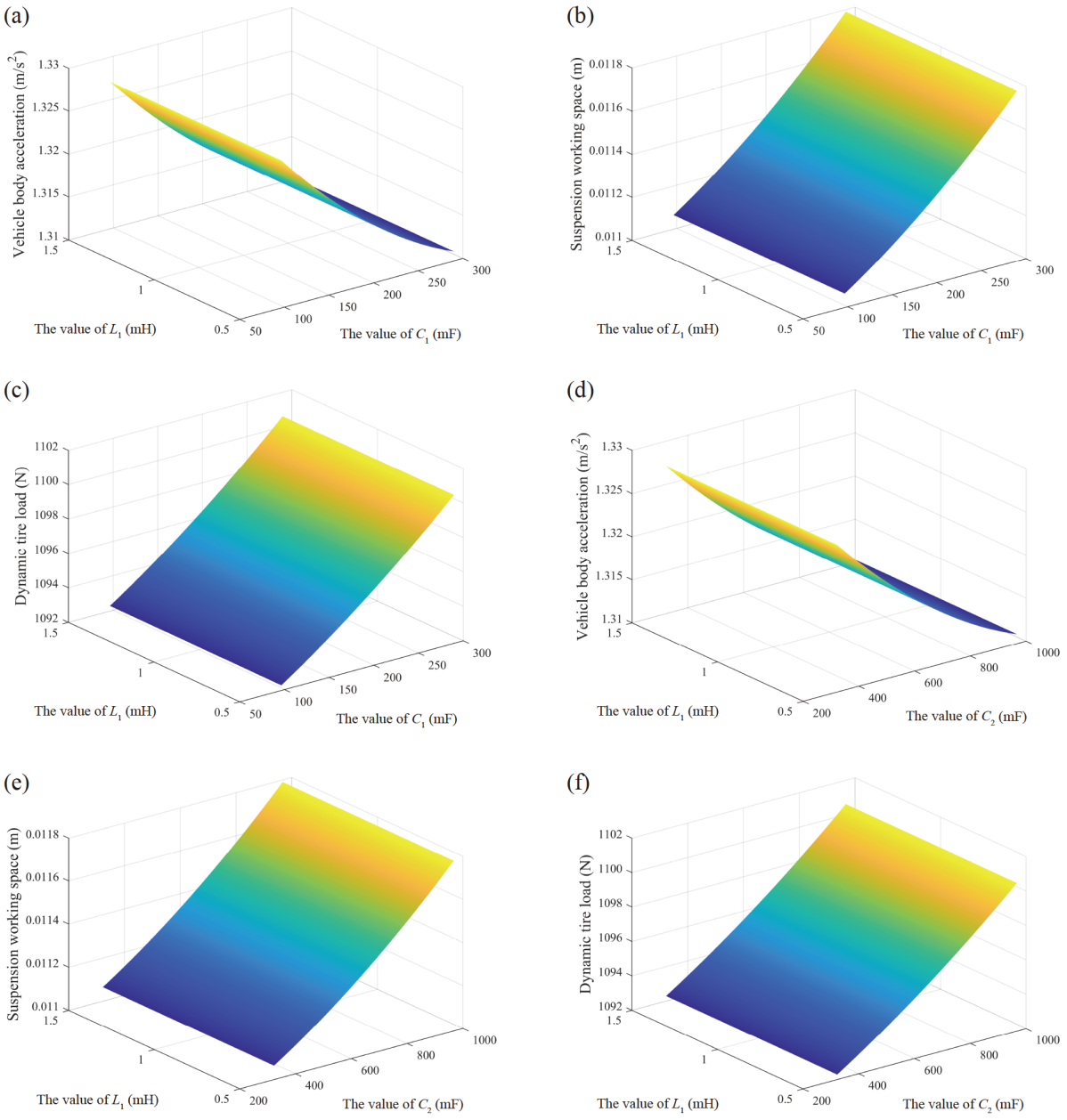

Figure 10 Influence of parameter variation of different types of energy storage components on suspension performance: (a) effect of C_1 and L_1 variation on body acceleration, (b) effect of C_1 and L_1 variation on suspension working space, (c) effect of C_1 and L_1 variation on dynamic tire load, (d) effect of C_2 and L_1 variation on body acceleration, (e) effect of C_2 and L_1 variation on suspension working space, and (f) effect of C_2 and L_1 variation on dynamic tire load.

and dynamic tire load increase with the increase of C_1 or C_2, and has no obvious relationship with the change of L_1. The variation range of the RMS values of the three evaluation indexes did not change greatly. In general, the parameter variation of the energy storage component combination had little influence on the suspension performance.

The bridge network contains both energy storage elements and energy dissipation elements. Then the R-C_1 and R-L_1 combinations are taken as examples to analyze the interaction between different types of elements and study the impact of parameter changes on suspension performance. The results are shown in Fig. 11.

Figure 11(a)-(c) shows the influence relationship of R and C_1 change on suspension, and the other pictures show the influence relationship of R and L_1 change on suspension. As can be seen from Fig. 11, the RMS value of body acceleration decreases with the increase of R but remains basically unchanged with the increase of C_1 or L_1. The RMS value of suspension working space and dynamic tire load increase with the increase of R, and slightly increases with the increase of C_1 or L_1. To further study the influence of energy consuming components on suspension performance, the output response of suspension when resistor parameters change is analyzed, and the results are shown in Fig. 12.

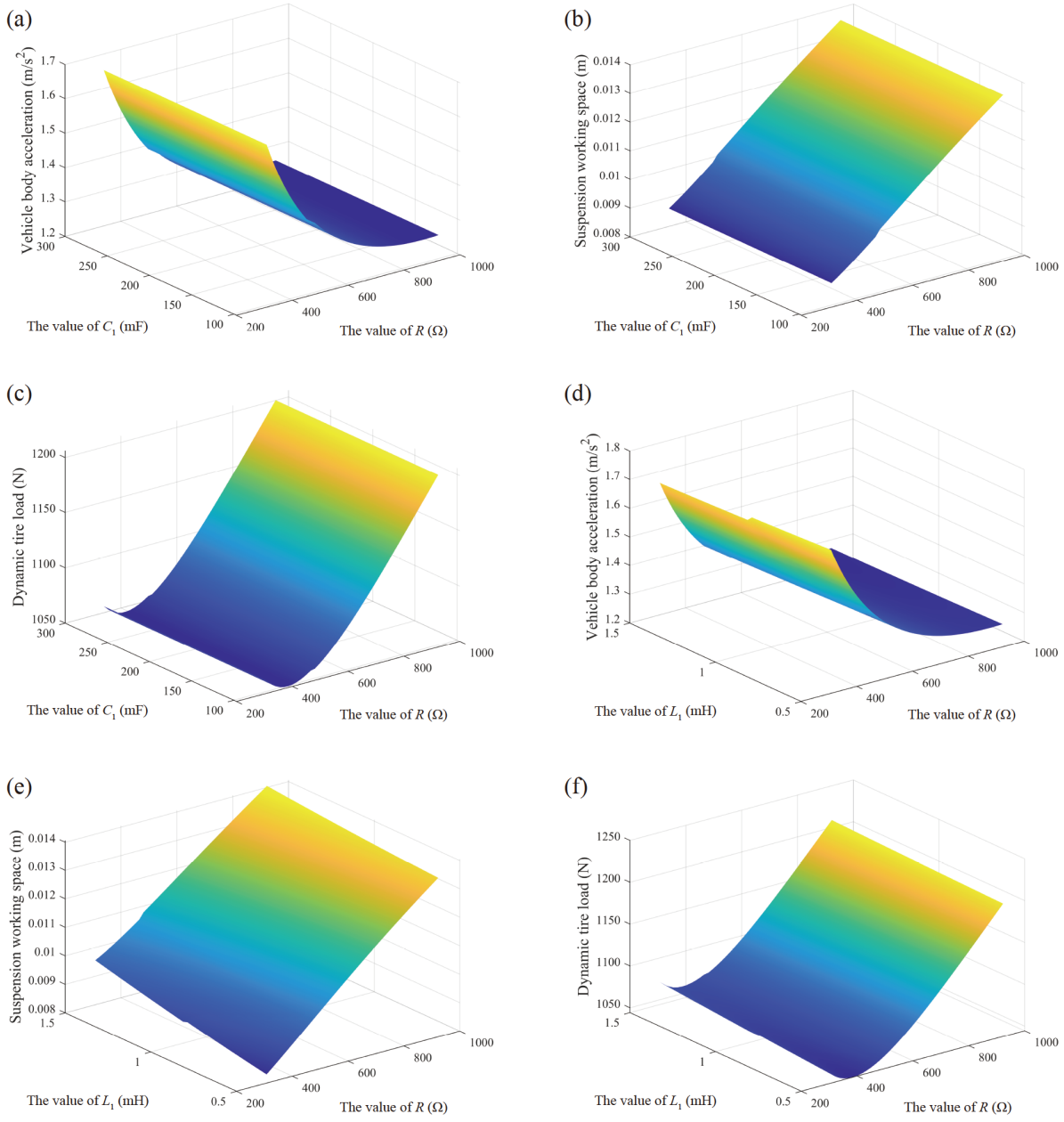

Figure 11 Influence of parameter changes of energy storage components and energy dissipating components on suspension performance: (a) effect of R and C_1 variation on body acceleration, (b) effect of R and C_1 variation on suspension working space, (c) effect of R and C_1 variation on dynamic tire load, (d) effect of R and L_1 variation on body acceleration, (e) effect of R and L_1 variation on suspension working space, and (f) effect of R and L_1 variation on dynamic tire load.

As can be seen from Fig. 12, the RMS value of body acceleration decreases with the increase of resistor parameters. The RMS value of suspension working space increases with the increase of resistor, and the RMS value of dynamic tire load first decreases and then increases with the increase of resistor. In terms of energy, when the energy consuming element takes a larger value, the input energy will be dissipated and absorbed at a faster speed. Then the energy transferred to the sprung mass becomes less, the body acceleration decreases and better riding comfort can be obtained. However, while energy consuming components absorb energy, there is still some energy in the energy storage elements. Even if the relationship between energy storage components and suspension output response is not very obvious, the existence of this part of the energy will affect the unsprung mass. That will increase the dynamic tire load, and affect the grounding and handling stability of the vehicle. Therefore, to suppress the negative effect of HMDV vertical vibration and reduce the dynamic tire load, it is necessary to take the appropriate resistor value. Thus the grounding of the vehicle could be improved based on ensuring the ride comfort.

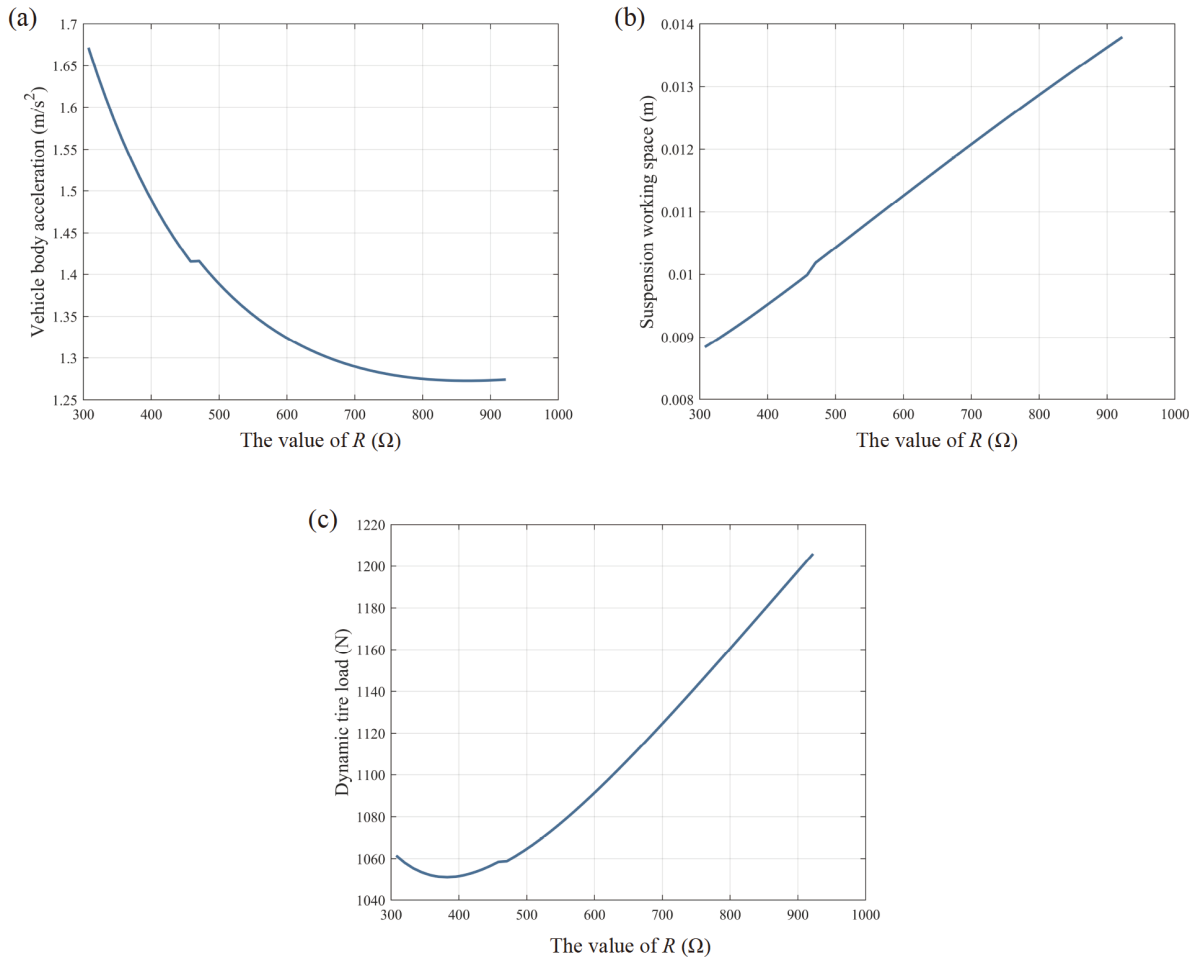

Figure 12 Influence of parameter changes of energy dissipating components on suspension performance: (a) effect of R variation on body acceleration, (b) effect of R variation on suspension working space, and (c) effect of R variation on dynamic tire load.

5. Conclusion

In this paper, the deterioration of dynamic tire load caused by the vertical vibration negative effect of HMDV is studied. The high order impedance function is used to suppress the negative effect of vertical vibration, and a bridge network structure is established. The biquartic impedance of an electrical network is equivalent to that of the mechanical network by a linear motor. The bridge network structure with 2 inductors, 2 capacitors, and 1 resistor is constructed from the perspective of forward structural analysis. Then the impedance function of different structures is analyzed by topological formulas. To improve the tire grounding, the optimization algorithm is used to find the best parameters corresponding to the bridge network structure. The simulation analysis shows that the strict biquartic impedance is better than the non-strict biquartic impedance. Compared with the conventional suspension, the RMS values of the dynamic tire load and suspension working space can be reduced by 10.76% and 18.10%, respectively. The body acceleration is also maintained to the same degree as that of the conventional suspension. The suspension with a bridge network can also suppress the vibration at low and high frequencies of HMDV. The Z_7 structure was selected as the research object to analyze the influence of parameter perturbations of different components on suspension performance. It was found that the parameter changes of energy storage components had a general effect on the improvement of suspension performance. The parameter variation of energy consuming components has a great influence on the performance of the suspension. Selecting the appropriate parameters for the bridge network structure can improve the grounding of the vehicle and keep the ride comfort to a good degree.

The mechatronic suspension using the bridge electrical network proposed in this paper only uses four energy storage elements and one energy dissipation element to achieve the biquartic impedance function. Compared to the implementation of series-parallel networks with high order impedance functions, the bridge network can be achieved with only 5 components. Compared to the bicubic impedance function containing five components, this paper

achieves a higher biquartic impedance by changing the type and quantity of components. In addition, this mechatronic suspension uses a linear motor and external circuit to simulate the impedance function. This reduces the space occupied by mechanical components, providing great convenience for the layout and maintenance of practical applications. The proposed analysis method provides a new idea for the suppression of the negative effects of vertical vibration of HMDV. It also provides a research direction for the realization and analysis of higher-order impedance functions. The types and connection modes of electrical elements proposed in this paper are only part of the electrical network. Future research will include different types and quantities of components, and based on simulation analysis, experiments are conducted to verify the simulation results.

Appendix

The expressions of the impedance functions of other bridge network structures are as follows:

$$\frac{1}{Z_2(s)}=\frac{A_2s^4+B_2s^3+C_2s^2+D_2s+E_2}{F_2s^4+G_2s^3+H_2s^2+I_2s+J_2}, \tag{A1}$$

$$\begin{cases} A_2=L_1L_2C_1C_2, \\ B_2=RC_1C_2(L_1+L_2), \\ C_2=L_1C_2+L_2C_1, \\ D_2=R(C_1+C_2), \\ E_2=1, \\ F_2=RL_1L_2C_1C_2, \\ G_2=L_1L_2(C_1+C_2), \\ H_2=R(L_1C_1+L_2C_2), \\ I_2=L_1+L_2, \\ J_2=R, \end{cases} \tag{A2}$$

$$\frac{1}{Z_4(s)}=\frac{A_4s^4+B_4s^3+C_4s^2+D_4s+E_4}{F_4s^4+G_4s^3+H_4s^2+I_4s+J_4}, \tag{A3}$$

$$\begin{cases} A_4=L_1L_2C_1C_2, \\ B_4=RL_1C_1C_2, \\ C_4=(L_1+L_2)(C_1+C_2), \\ D_4=R(C_1+C_2), \\ E_4=0, \\ F_4=RL_1L_2C_1C_2, \\ G_4=L_1L_2C_1, \\ H_4=RL_1(C_1+C_2)+RL_2C_2, \\ I_4=L_1+L_2, \\ J_4=R, \end{cases} \tag{A4}$$

$$\frac{1}{Z_5(s)}=\frac{A_5s^4+B_5s^3+C_5s^2+D_5s+E_5}{F_5s^4+G_5s^3+H_5s^2+I_5s+J_5}, \tag{A5}$$

$$\begin{cases} A_5=L_1L_2C_1C_2, \\ B_5=RL_1C_1C_2, \\ C_5=L_1C_2+L_2(C_1+C_2), \\ D_5=R(C_1+C_2), \\ E_5=1, \\ F_5=RL_1L_2C_1C_2, \\ G_5=L_1L_2C_1, \\ H_5=R(L_1+L_2)(C_1+C_2), \\ I_5=L_1+L_2, \\ J_5=0, \end{cases} \tag{A6}$$

$$\frac{1}{Z_6(s)}=\frac{A_6s^4+B_6s^3+C_6s^2+D_6s+E_6}{F_6s^4+G_6s^3+H_6s^2+I_6s+J_6}, \tag{A7}$$

$$\begin{cases} A_6=L_1L_2C_1C_2, \\ B_6=RL_2C_1C_2, \\ C_6=C_1(L_1+L_2)+L_1C_2, \\ D_6=R(C_1+C_2), \\ E_6=1, \\ F_6=RL_1L_2C_1C_2, \\ G_6=L_1L_2(C_1+C_2), \\ H_6=RL_1(C_1+C_2)+RL_2C_2, \\ I_6=L_2, \\ J_6=R, \end{cases} \tag{A8}$$

$$\frac{1}{Z_8(s)}=\frac{A_8s^4+B_8s^3+C_8s^2+D_8s+E_8}{F_8s^4+G_8s^3+H_8s^2+I_8s+J_8}, \tag{A9}$$

$$\begin{cases} A_8=L_1L_2C_1C_2, \\ B_8=RC_1C_2(L_1+L_2), \\ C_8=L_1(C_1+C_2)+L_2C_1, \\ D_8=RC_2, \\ E_8=1, \\ F_8=0, \\ G_8=L_1L_2(C_1+C_2), \\ H_8=R(L_1+L_2)(C_1+C_2), \\ I_8=L_2, \\ J_8=R, \end{cases} \tag{A10}$$

$$\frac{1}{Z_9(s)}=\frac{A_9s^4+B_9s^3+C_9s^2+D_9s+E_9}{F_9s^4+G_9s^3+H_9s^2+I_9s+J_9}, \tag{A11}$$

$$\begin{cases} A_9 = 0, \\ B_9 = RC_1C_2(L_1+L_2), \\ C_9 = (C_1+C_2)(L_1+L_2), \\ D_9 = RC_1, \\ E_9 = 1, \\ F_9 = RL_1L_2C_1C_2, \\ G_9 = L_1L_2(C_1+C_2), \\ H_9 = RL_1(C_1+C_2)+RL_2C_1, \\ I_9 = L_2, \\ J_9 = R. \end{cases} \tag{A12}$$

Conflict of interest *On behalf of all authors, the corresponding author states that there is no conflict of interest.*

Author contributions ***Xiaofeng Yang:*** *Conceptualization, Resources, Funding acquisition, Revised the final version.* ***Yan Yan:*** *Formal analysis, Investigation, Visualization and wrote the first draft of the manuscript.* ***Yujie Shen:*** *Writing – review and editing, Funding support, Revised and edited the final version.* ***Xiaofu Liu:*** *Project administration, Funding acquisition and helped organize the manuscript.* ***Zhipeng Wang:*** *Funding support, Data curation and maintain research data.*

Acknowledgements *This work was supported by the National Natural Science Foundation of China (Grant No. 52072157), Innovation Center of Modern Agricultural Equipment (Grant No. XTCX2022), State Key Laboratory of Advanced Design and Manufacturing Technology for Vehicle (Grant No. 82315004), Qing Lan Project of Jiangsu Province, Young Elite Scientists Sponsorship Program by CAST (Grant No. 2022QNRC001), and China Postdoctoral Science Foundation (Grant Nos. 2024T171048 and 2024M753653).*

1 D. Mohanraj, J. Gopalakrishnan, B. Chokkalingam, and L. Mihet-Popa, Critical aspects of electric motor drive controllers and mitigation of torque ripple—review, IEEE Access **10**, 73635 (2022).
2 J. Wang, S. Gao, Y. Qiang, M. Xu, C. Guan, and Z. Zhou, Structural topology and dynamic response analysis of an electric torque vectoring drive-axle for electric vehicles, Automot. Innov. **5**, 164 (2022).
3 Z. X. Li, C. L. Liu, X. Y. Song, and C. C. Wang, Vibration suppression of hub motor electric vehicle considering unbalanced magnetic pull, Proc. Inst. Mech. Eng. **235**, 3185 (2021).
4 W. H. Yang, Z. F. Fang, K. D. He, in Study on the Influence of Hub Motor on Ride Comfort of Electric Vehicle: Proceedings of 2017 International Conference on Material Science, Energy and Environmental Engineering, Xi'an, 2017.
5 X. Chen, Y. Leng, F. Sun, X. Su, S. Sun, and J. Xu, Passive vibration reduction performance of a triple-magnet magnetic suspension dynamic vibration absorber under sinusoidal excitation, Acta Mech. Sin. **39**, 522286 (2023).
6 X. Li, A. Mojahed, L. Q. Chen, L. A. Bergman, and A. F. Vakakis, Shock response mitigation of a large-scale structure by modal energy redistribution facilitated by a strongly nonlinear absorber, Acta Mech. Sin. **38**, 121464 (2022).
7 C. N. Liu, S. K. Lai, Y. Q. Ni, and L. Chen, Dynamic modeling and analysis of a physics-driven strategy for vibration control of railway vehicles, Veh. Syst. Dyn. (2024).
8 Y. Yang, C. Liu, L. Chen, and X. Zhang, Phase deviation of semi-active suspension control and its compensation with inertial suspension, Acta Mech. Sin. **40**, 523367 (2024).
9 G. P. Sreenivasan, and M. M. Keppanan, Analytical approach for the design of convoluted air suspension and experimental validation, Acta Mech. Sin. **35**, 1093 (2019).
10 Y. Shen, D. Qiu, X. Yang, J. Chen, Y. Guo, and T. Zhang, Vibration isolation performance analysis of a nonlinear fluid inerter-based hydro-pneumatic suspension, Int. J. Struct. Stab. Dyn..
11 L. Meng, Y. Zou, Y. Qin, and Z. Hou, A new electric wheel and optimization on its suspension parameters, Proc. Inst. Mech. Eng. Part D-J. Automobile Eng. **234**, 2759 (2020).
12 Z. Li, X. Song, X. Chen, H. Xue, and G. Ruta, Dynamic characteristics analysis of the hub direct drive-air suspension system from vertical and longitudinal directions, Shock Vib. **2021(1)**, 8891860 (2021).
13 Y. Liu, L. Chen, T. Cai, W. Sun, X. Xu, and S. Wang, Dual-pump control algorithm of two-speed powershift transmissions in electric vehicles, Automot. Innov. **5**, 57 (2022).
14 Y. Yu, Z. Li, Y. Zhou, and X. Wang, A nonlinear model predictive control for air suspension in hub motor electric vehicle, Proc. Inst. Mech. Eng. Part D-J. Automobile Eng. (2024).
15 M. C. Smith, Synthesis of mechanical networks: The inerter, IEEE Trans. Automat. Contr. **47**, 1648 (2002).
16 Y. Shen, J. Hua, W. Fan, Y. Liu, X. Yang, and L. Chen, Optimal design and dynamic performance analysis of a fractional-order electrical network-based vehicle mechatronic ISD suspension, Mech. Syst. Signal Process. **184**, 109718 (2023).
17 Y. Wang, P. Wang, H. Meng, and L. Q. Chen, Nonlinear vibration and dynamic performance analysis of the inerter-based multi-directional vibration isolator, Arch Appl. Mech. **92**, 3597 (2022).
18 Y. Shen, A. Chen, F. Du, X. Yang, Y. Liu, and L. Chen, Performance enhancements of semi-active vehicle air ISD suspension, Proc. Inst. Mech. Eng. Part D-J. Automobile Eng. (2024).
19 J. Nie, Y. Zhao, X. Zhang, and T. Zhang, Design and test of lateral interconnected hydro-pneumatic ISD suspension, Proc. Inst. Mech. Eng. Part D-J. Automobile Eng. **238**, 633 (2024).
20 Y. Shen, M. Jia, X. Yang, Y. Liu, and L. Chen, Vibration suppression using a mechatronic PDD-ISD-combined vehicle suspension system, Int. J. Mech. Sci. **250**, 108277 (2023).
21 X. Yang, H. Song, Y. Shen, and Y. Liu, Study on adverse effect suppression of hub motor driven vehicles with inertial suspensions, Proc. Inst. Mech. Eng. Part D-J. Automobile Eng. **236**, 767 (2022).
22 Y. Li, X. Yang, Y. Shen, Y. Liu, and W. Wang, Optimal design and dynamic control of the HMDV inertial suspension based on the ground-hook positive real network, Adv. Eng. Software **171**, 103171 (2022).
23 X. Yang, T. Zhang, Y. Shen, Y. Liu, V. C. Bui, and D. Qiu, Tradeoff analysis of the energy-harvesting vehicle suspension system employing inerter element, Energy **308**, 132841 (2024).
24 Y. Wang, B. Xu, and H. Meng, Enhanced vehicle shimmy performance using inerter-based suppression mechanism, Commun. Nonlinear Sci. Numer. Simul. **130**, 107800 (2024).
25 F. C. Wang, and H. A. Chan, Vehicle suspensions with a mechatronic network strut, Veh. Syst. Dyn. **49**, 811 (2011).
26 A. Gonzalez-Buelga, L. R. Clare, S. A. Neild, J. Z. Jiang, and D. J. Inman, An electromagnetic inerter-based vibration suppression device, Smart Mater. Struct. **24**, 055015 (2015).
27 Y. J. Shen, D. H. Shi, L. Chen, Y. L. Liu, and X. F. Yang, Modeling and experimental tests of hydraulic electric inerter, Sci. China Tech. Sci. **62**, 2161 (2019).
28 R. Bott, and R. J. Duffin, Impedance synthesis without use of transformers, J. Appl. Phys. **20**, 816 (1949).
29 J. Z. Jiang, and M. C. Smith, Series-parallel six-element synthesis of biquadratic impedances. IEEE Tech. Circuits-I. **59**, 2543 (2012).
30 J. Z. Jiang, and M. C. Smith, Regular positive-real functions and five-element network synthesis for electrical and mechanical networks, IEEE Trans. Automat. Contr. **56**, 1275 (2011).
31 K. Wang, M. Z. Q. Chen, and Y. Hu, Synthesis of biquadratic impedances with at most four passive elements, J. Franklin Inst. **351**, 1251 (2014).
32 S. Y. Zhang, J. Z. Jiang, H. L. Wang, and S. Neild, Synthesis of essential-regular bicubic impedances, Circuit Theor. Apps **45**, 1482

(2017).
33 T. H. Hughes, Minimal series-parallel network realizations of bicubic impedances, IEEE Trans. Automat. Contr. **65**, 4997 (2020).
34 R. H. Pantell, A new method of driving-point impedance synthesis, Proc. Inst. Radio Eng. **42**, 861 (1954).
35 M. Z. Q. Chen, K. Wang, C. Y. Li, and G. R. Chen, in Realizations of biquadratic impedances as five-element bridge networks containing one inductor and one capacitor: Proceedings of the 33rd Chinese Control Conference, Nanjing, 2014.
36 K. Wang, and M. Z. Q. Chen, Passive mechanical realizations of bicubic impedances with no more than five elements for inerter-based control design, J. Franklin Inst. **358**, 5353 (2021).
37 W. Sun, Y. Li, J. Huang, and N. Zhang, Vibration effect and control of in-wheel switched reluctance motor for electric vehicle, J. Sound Vib. **338**, 105 (2015).
38 B. Fahimi, A. Emadi, and R. B. Sepe, Four-quadrant position sensorless control in SRM drives over the entire speed range, IEEE Trans. Power Electron. **20**, 154 (2005).
39 I. Husain, and M. Ehsani, in Torque ripple minimization in switched reluctance motor drives by PWM current control: Proceedings of 1994 IEEE Applied Power Electronics Conference and Exposition (ASPEC), Orlando, 1994.
40 Z. Z. Ye, T. W. Martin, and J. C. Balda, in Modeling and nonlinear control of a switched reluctance motor to minimize torque ripple: Proceedings of 2000 IEEE International Conference on Systems, Man and Cybernetics, Nashville, 2000.
41 S. Seshu, and M. B. Reed, Linear Graphs and Electrical Networks (Addison-Wesley, Boston, 1961).

基于桥式网络的HMDV悬架优化设计与动态性能分析

杨晓峰, 闫炎, 沈钰杰, 刘骁夫, 王志鹏

摘要 本文设计了一种基于桥式网络的新型机电悬架, 用于解决轮毂电机驱动汽车(HMDV)因簧下质量增加而造成的垂向振动负效应问题. 首先基于两个电容元件、两个电感元件和一个电阻元件来构建桥式网络, 并通过结构化方法对其阻抗函数进行正向分析. 然后建立1/4 HMDV模型, 使用模式搜索算法优化电网络中的元件参数, 并进一步分析在最优结构下元件参数摄动对悬架输出响应的影响. 结果表明, 所提出的桥式电网络能够实现双四次的阻抗函数, 并能通过直线电机等效为机械阻抗. 与传统悬架相比, 轮胎动载荷与悬架动行程的均方根值分别降低了10.76%和18.10%. 簧下质量在低频和高频处的振动得到抑制, 有效提升了车辆的接地性和操纵稳定性.